Implementation of DVB-S2X Super-Frame Format 4 for Wideband Transmission

Christian Rohde[1]([✉]), Holger Stadali[1], Javier Perez-Trufero[2], Simon Watts[2], Nader Alagha[3], and Riccardo De Gaudenzi[3]

[1] Fraunhofer Institute for Integrated Circuits (IIS), Am Wolfsmantel 33, 91058 Erlangen, Germany
{Christian.Rohde,Holger.Stadali}@iis.fraunhofer.de
http://www.iis.fraunhofer.de/dvbs2x
[2] Avanti Communications, Cobham House, 20 Black Friars Lane, London, UK
{javier.pereztrufero,simon.watts}@avantiplc.com
[3] European Space Agency (ESA), ESA ESTEC, Noordwijk, The Netherlands
{Nader.Alagha,Riccardo.de.Gaudenzi}@esa.int

Abstract. Recently the extension of the digital video broadcasting second generation standard for transmission over satellite (DVB-S2) has been finalized in order to achieve a higher spectral efficiency without introducing fundamental changes to the complexity and structure of the common DVB-S2 standard [1]. Therefore, this extension is termed DVB-S2X. In this paper, we focus on a more powerful physical layer frame structure, known as Super-Frame (SF), which has been adopted as optional waveform container in Annex E of the DVB-S2X specification [2]. The paper provides insights to capabilities of the SF structure in support of emerging system applications. Analytical results of the SF performance are complemented by the performance results obtained from an end-to-end testbed implementing SF format 4, which is optimized for wideband transmission and very low SNR reception conditions. The testbed includes prototype design of modulator and demodulator featuring the SF generation and detection capability. The prototype devices are able to operate at a wide range of signal-to-noise ratios and at high symbol rates. This design represents the basis for planned over-the-air tests using a single wideband satellite transponder to demonstrate the feasibility of transmitting and receiving 1 Gbit/s.

Keywords: Digital video broadcasting (DVB) · Super-frame synchronization · Wideband transmission · Very low SNR · Broadcast satellite systems (BSS)

1 Introduction to DVB-S2X Super-Framing

The recently introduced DVB-S2X standard [2] keeps the physical layer frame (PLFRAME) structure from DVB-S2 [1]. It results in variable frame size depending on chosen modulation and coding (MODCOD) and pilots On/Off signaled

by the slightly modified physical layer header (PLH). The key innovations are new MODCODs for finer granularity in spectral efficiency and an extended SNR range, lower roll-offs compared to DVB-S2, a special frame for very low signal-to-noise ratio (VL-SNR) burst mode reception, and channel bonding to allow coordinated data spreading over different signals [4].

The use of variable coding and modulation (VCM) and adaptive coding and modulation (ACM) schemes may introduce additional complexity at the receiver due to the time-variant PLFRAME size. Furthermore, the non-constant PLFRAME size dramatically complicates the implementation of techniques such as multi-user multiple-input multiple-output (MU-MIMO) transmission over satellite [5] or beam-hopping/-switching in multi-spot-beam satellite systems [6]. Therefore, the SF concept has been included to the DVB-S2X specification providing additional regular framing structures in order to enable these and future techniques as well as to support receiver synchronization in severe channel conditions [3].

1.1   Common Components of Super-Frames

The SF concept follows a simple rule to provide a common container that allows hosting different format-specific contents as illustrated in Fig. 1. In essence, each SF consists of exactly 612,540 physical layer symbols that are split among the following fields:

– Start of SF (SOSF) is composed of 270 symbols containing a known sequence, chosen from a set of orthogonal Walsh-Hadamard (WH) sequences, to be used to detect the SF and to mark the start of the SF.
– SF format indicator (SFFI) consists of 450 symbols, embedding 4 bits of signaling information (robustly coded and spread over 450 symbols) that is used to identify 16 distinct SF formats.
– A common data/signaling field of 611,820 symbols can be allocated in several different ways to the actual physical layer frames according to the SFFI.
– The SF aligned scrambling sequence that is applied to the entire length of the SF symbols, with possibility of individual scrambling for signaling and payload elements. The scrambling sequence could also vary per beam in a multi-beam system.

All SF formats share these common elements and a constant SF length, independent of the container content. A periodic repetition of the SF helps the demodulator to perform the detection and the synchronization operation. Furthermore, from the SF format that is decoded from the SFFI, the receivers can identify the content of the SF. This allows the receivers to decode only the desired formats and to discard other SF formats while maintaining the synchronization to the SF structure and removing the carrier and symbol clock uncertainties.

Currently, five different SF formats are specified in DVB-S2X Annex E [2] to be carried in the SF container:
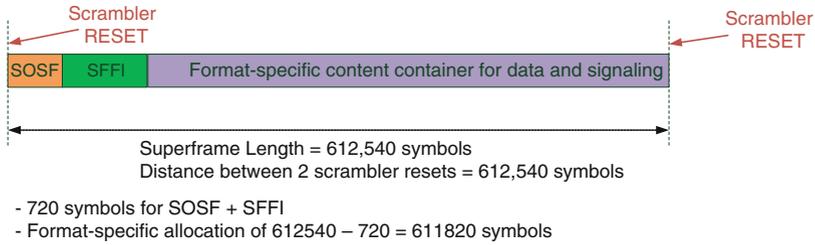
Fig. 1. Common structure of the super-frame of DVB-S2X Annex E [2].

- Format 0: DVB-S2X but with SF-aligned pilots and including the new VL-SNR frame for VL-SNR burst-mode reception
- Format 1: Legacy support of DVB-S2 but with SF-aligned pilots
- Format 2 and 3: Bundled PLFRAME formats suitable for precoding and beam-hopping applications
- Format 4: Flexible multi-purpose format optimized for wideband transmission and large SNR range

1.2   Format-Specific Components of Format 4

SF format 4 provides support for wideband carrier transmission since each PLH carries information about the PLFRAME time slicing number (or stream ID) that could be used at the receiver to apply PLFRAME filtering to decode only a target subset of all PLFRAMEs. This format is also suitable for VL-SNR operation due to the availability of PLFRAME spreading factors 2 and 5.

Format 4 offers four different PLH protection levels which are signaled by the super-frame header (SFH):

- Level 0: Standard protection (size 2 slots) using BPSK modulation and overall code rate 1/10
- Level 1: Robust protection (size 4 slots) using BPSK modulation and spreading 2 leading to an overall code rate 1/20
- Level 2: Very robust protection (size 10 slots) using BPSK modulation and spreading 5 leading to an overall code rate 1/50
- Level 3: High efficiency mode (size 1 slot) using QPSK modulation and overall code rate 1/8.75 due to puncturing

The signaling of the PLH robustness level as well as a pointer to the first PLH in the SF enable the support of VCM/ACM transmission scenarios, which includes VL-SNR applications but also high efficiency signaling for the high SNR and high throughput case. Although the protection level can change on a per SF basis, which is advantageous for traffic shaping, the most optimized PLH protection always assures such that each served receiver (with individual SNR conditions) in a SF can perform successful PLH tracking.

Finally, four different dummy frame types are defined in addition to the conventional DVB-S2 dummy frame. The four types result from the combinations of "arbitrary or deterministic content" and "regular size dummy frame or dummy frame termination at end of SF". The first criterion exploits that the signaled MODCOD of the PLH has to be respected for the dummy frame generation, which shall provide a large variety of (non-linear) channel estimation means suitable for application of predistortion techniques. The second criterion determines whether a dummy frame has regular length according to the signaled MODCOD or terminates with the end of the SF (dynamic SF padding), which is of value for SF-wise processing as required, e.g., for beam-hopping.

2   Super-Frame Synchronization Performance

The common elements of the SF (SF length, SOSF and SFFI structure) allow common processing techniques for SF detection and frame synchronization independently of the actually transmitted SF content format. A common SF detection processor solely relies on the structure as presented in Fig. 1 but needs a priori knowledge of the SOSF Walsh-Hadamard sequence index and the SF scrambler configuration. The SF synchronization can be further enhanced by utilizing the SFFI underlying spreading sequences structure.

A reliable detection of the start of SF is essential for the overall synchronization and operation of receivers adopting SF structure. Accordingly, robust detection techniques are discussed in the following to allow operation at VL-SNR and in the presence of carrier frequency and clock frequency uncertainties.

2.1   Super-Frame Detection Algorithms

The SF detection relies on correlation algorithms, similar to many other frame synchronization solutions. In the following sub-sections, different algorithms for correlation peak detection are introduced and compared in terms of robustness and detection performance taking into account channel imperfections.

Conventional Full Correlation. A conventional approach for SF detection is to carry out cross-correlation of the receiver input samples and the full-length reference sequence and compare to a threshold for correlation peak detection. Let $c[k]$ denote the correlator output at time instant k. We use the Euclidian norm of the correlator function for correlation peak analysis, i.e.

$$b[k] = \mathrm{abs}(c[k])^2 = \mathrm{Re}\left\{c[k]\right\}^2 + \mathrm{Im}\left\{c[k]\right\}^2. \tag{1}$$

We also assume an additive white Gaussian noise (AWGN) present at the correlator input. Apart from a correlation peak, the correlator output $c[k]$ as a time-discrete random variable will have Gaussian distribution [7]. Thus, the noise component of $b[k]$ has a Chi-square distribution with two degrees of freedom. This noise component is defined as $n_b[k]$ with probability density function

$$f(n_b, \sigma_{n_b}) = \frac{1}{2\sigma_{n_b}^2} \cdot \mathrm{e}^{-\frac{n_b}{2\sigma_{n_b}^2}} \tag{2}$$

for values $n_b \geq 0$. Herein, $\sigma_{n_b}^2$ denotes the variance of the noise component. Note that this also holds in case of only noise at the correlator input in absence of a signal, which results in a reduced $\sigma_{n_b}^2$. To calculate the false alarm probability $Pr(FA)$, i.e. the probability that a correlation noise sample is above the threshold instead of the true correlation peak, we use

$$Pr(FA) = Pr(n_b > b_{\mathrm{thresh}}) = 1 - Pr(n_b \leq b_{\mathrm{thresh}})$$
$$= 1 - \int_0^{b_{\mathrm{thresh}}} f(n_b, \sigma_{n_b}) \, \partial n_b = \mathrm{e}^{-\frac{b_{\mathrm{thresh}}}{2\sigma_{n_b}^2}} . \tag{3}$$

This represents the probability that a noise sample $n_b[k]$ occurs at any sampling instant k, which is greater than a threshold b_{thresh}. Thus, we can calculate from (3) the appropriate threshold for a target false alarm probability $Pr(FA_{\mathrm{target}})$ by

$$b_{\mathrm{target}} = -\ln\left(Pr(FA_{\mathrm{target}})\right) \cdot 2\sigma_{n_b}^2. \tag{4}$$

Consequently, a scaling factor $S = -\ln(Pr(FA_{\mathrm{target}}))$ results from the target false alarm probability. Knowing that the correlation noise within $c[k]$ is Gaussian, an estimation of the actual value of $2\sigma_{n_b}^2$ is achieved by averaging over $b[k]$. Thus, an adaptive threshold results as

$$b_{\mathrm{thresh}}[k] = S \cdot \mathrm{mean}(b[k]) \approx S \cdot 2\sigma_{n_b}^2, \tag{5}$$

which meets b_{target} on average. This is known as Constant False Alarm Rate (CFAR) correlator peak detector [8].

Note that the operator $\mathrm{mean}(\cdot)$ is averaging the peak detector input samples except for the ones for which the value exceeds the threshold i.e. $b[k] > b_{\mathrm{thresh}}[k - k_{\mathrm{guard}}]$ with e.g. $k_{\mathrm{guard}} = 2$ or 3. This is to avoid misdetection because the correlation peak would already be part of the average for $k_{\mathrm{guard}} = 0$ [9].

Subblock-Based Abs-Square Algorithm. The performance of full-length cross-correlation algorithm degrades considerably due to carrier frequency offset (CFO). Even in the presence of small CFOs, which are very likely to occur during the acquisition phase, the performance degradation is quite high. With increasing CFOs the correlation peak value decreases, which leads to a higher probability of misdetecting valid peaks. The correlation loss gets larger for longer sequences like the 270 symbols of the SOSF or even worse in case of the 720 symbols SOSF+SFFI length.

As a remedy, we divide the correlation window into SB subblocks. In other words, the correlator is applied to SB subblocks of the SOSF, so that each correlation subblock has a length of $L_{SB} = \lfloor \text{SOSF length}/SB \rfloor$. Consequently, $c_1[k]$ is the result of correlating the input signal with the first part of the SOSF

and $c_2[k]$ is related to the second part and so on. Note, that this splitting is related to the original full length correlation by

$$c[k] = \sum_{i=1}^{SB} c_i[k - (SB - i) \cdot L_{SB}] = \sum_{i=1}^{SB} c_i'[k], \tag{6}$$

which represents also a common method to parallelize a correlation. For the sake of easier notation the variable $c_i'[k]$ already includes the necessary delays.

As a subblock combining scheme, we can derive the absolute square of each subblock correlation result by

$$b_{\text{Abs-Square}}[k] = \sum_{i=1}^{SB} \text{abs}\left(c_i'[k]\right)^2. \tag{7}$$

This represents a straight forward extension of the previous algorithm for the full correlation but with phase removal. Accordingly, the noise component in $b_{\text{Abs-Square}}[k]$ again features a Chi-Square distribution but here with $2 \cdot SB$ degrees of freedom. Thus, the false alarm probability is computed as [7]:

$$Pr(FA) = 1 - Pr(b_{\text{Abs-Square}}[k]) > b_{\text{thresh}}) = \text{e}^{-\frac{b_{\text{thresh}}}{2\sigma_{n_b}^2}} \cdot \sum_{k=0}^{SB-1} \frac{1}{k!} \cdot \left(\frac{b_{\text{thresh}}}{2\sigma_{n_b}^2}\right)^k. \tag{8}$$

In analogy to (5), we calculate the detection threshold by

$$b_{\text{thresh}} = S \cdot \text{mean}(b_{\text{Abs-Square}}[k]) \approx S \cdot SB \cdot 2\sigma_{n_b}^2. \tag{9}$$

This estimate enables to insert into (8), which yields

$$Pr(FA) = \text{e}^{-S \cdot SB} \cdot \sum_{k=0}^{SB-1} \frac{1}{k!} \cdot (S \cdot SB)^k. \tag{10}$$

Therefore, the scaling factor S can be determined for a given target $Pr(FA)$ and number of subblocks SB with iterative methods.

Subblock-based Cross-Correlation Algorithm (XCorr). An alternative subblock combining scheme is based on conjugate complex multiplication of the subblock correlation results in analogy to the differential post integration method [10]. The scheme is abbreviated as XCorr and defined by

$$b_{\text{XCorr}}[k] = \text{abs}\left(\sum_{i=1}^{SB-1} c_i'[k] \cdot c_{i+1}'^*[k]\right). \tag{11}$$

Due to the cross-correlation of the subblock correlation results, phase rotations due to CFO is transformed to a common delta phase, which enables a coherent summation of the cross-correlation results. In [10], $Pr(FA)$ is calculated for a given threshold but unfortunately there is no simple closed form expression of the threshold calculation for a given $Pr(FA)$ target. In order to determine a CFA rate, the scaling factor S in our case was determined empirically from the analysis of the noise histogram at a given target $Pr(FA)$.

Simulation Results. In order to analyze the impact of the CFO on the correlation peak detection performance, we first assume perfect symbol timing synchronization. Further below, we will drop this assumption to sketch a cold-start acquisition. We compare the following configurations:

– Full Corr. (270): Full Correlation w.r.t. the 270 symbols of the SOSF is applied, which is independent of the SFFI content by disregarding the SFFI.
– Full Corr. (720): Full Correlation w.r.t. the 720 symbols of SOSF+SFFI is applied, which either assumes a single target SFFI content or is realized with 16 parallel instances according to the 16 different SFFI code-words.
– Abs-Square (48 SBs): In order to exploit the SFFI structure (spreading by a factor of 30) for information removal, a subblock size of 15 symbols is selected for further analysis to ease the comparison with the XCorr algorithm. Here, the abs-operation performs information removal from the SFFI. This yields in total $18 + 30 = 48$ SBs from SOSF+SFFI for evaluation.
– XCorr (33 SBs): The maximum subblock size of the XCorr algorithm is here 15 symbols because of the pairwise conjugate complex multiplication of subblock correlation results for SFFI information removal. Although this yields 48 SBs from SOSF+SFFI, the SFFI information removal is limited to conjugate complex multiplication of disjoint pairs of subblock correlation results, which finally leads to an effective number of 15 SBs from the SFFI. This means in total $18 + 15 = 33$ SBs.

The rather small subblock size of 15 symbols shall enhance the CFO robustness. Note that a general XCorr SB size optimization w.r.t. SNR maximization under CFO is given by the so-called CHILD rule [10]: Choose the SB size close to $3/(8\nu)$ with the relative CFO $\nu = \Delta f \cdot T$. A worst-case CFO of $\nu = 0.02$ yields 18.75, which is already quite close to the chosen SB size.

The two subblock-related algorithms exploit the SFFI structure in a non data-aided (NDA) fashion opposed to the algorithm Full Corr. (720), where up to 16 parallel correlators each of 720 symbols length can be required due to the unknown SFFI sequence.

In Fig. 2, peak detection performance is shown versus E_s/N_0 for the described algorithms and different relative values of CFO. In all cases, a $Pr(FA) = 10^{-5}$ is targeted. This corresponds to 6 false peak detections on average per SF. However, due to the SF regular pattern, these false alarms can be easily discarded since their occurrence distance does not match the length of the SF. In fact, the distance between two consecutive SOSF or SOSF+SFFI detections shall be very close to an integer multiple of the SF length. The uncertainty is mainly due to potential symbol slips of a timing loop that is typically a very small portion compared to the SF length. Following the same logic, the regularity of SF structure also helps to compensate for occasional missing the peak detection since the occurring time of the start of SF can be predicted from previous SFs.

Figure 2 illustrates the sensitivity of the peak detector using full correlation algorithms to CFO values of 0.01 and 0.02. As shown in Fig. 2 the two
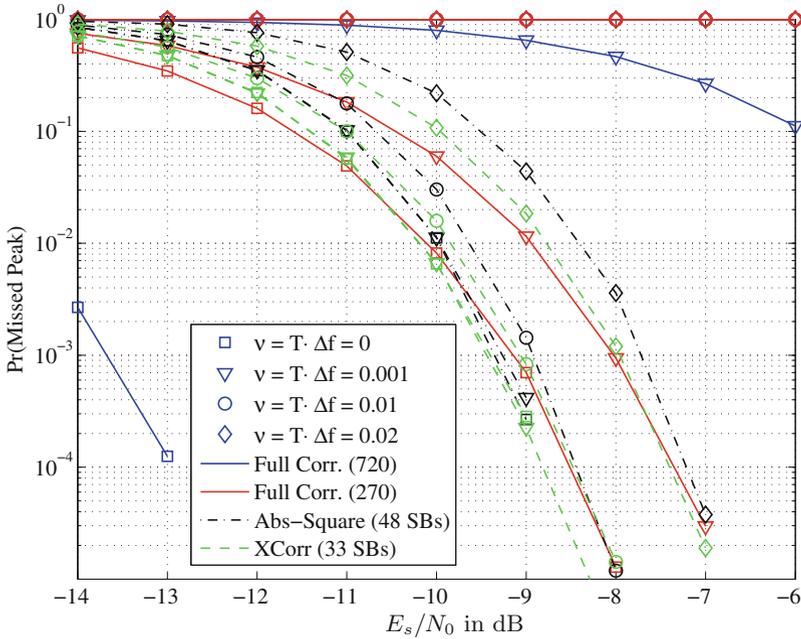
Fig. 2. $Pr(MP)$ versus E_s/N_0 of different algorithms with target $Pr(FA) = 10^{-5}$.

subblock-based algorithms (Abs-Square and XCorr) outperform the full correlation algorithms with a slight advantage for the XCorr one. Nevertheless, even the subblock-based algorithms show some notable degradation at CFO of $\nu = 0.02$.

2.2   Algorithms for SF-aided Timing Synchronization

Especially under VL-SNR conditions and low roll-offs as well as uncompensated sampling frequency offset (SFO) and CFO, a timing loop scheme [11] cannot converge properly. As a remedy, one can first start SF-detection which would suffer from the arbitrary sample timing. Thus, we describe an enhanced detection technique to maintain at 1 sample per symbol processing while tolerating the initial sample timing inaccuracy. The proposed approach implements two parallel SB related peak detection instances, instance A and B. Instance A performs best in case of sampling phase $\tau = 0$ and instance B aims for regenerating a high correlation result under the worst-case sampling phase offset of $\tau = 0.5$. Once a correlation peak grid is found, an estimate for the SFO can be calculated from the correlation peak distance and forwarded to the then activated timing loop for initialization. This provides significant support in VL-SNR configuration of the timing loop [12].

The hybrid or dual processing approach introduces additional evaluation logic after the two instances. Finally, the two hybrid or dual processing schemes are:

– Hybrid Abs-Square algorithm related processing:
  Instance A: $b_{\text{Abs-Square,A}}[k] = \sum_{i=1}^{SB} \text{abs}(c_i'[k])^2$
  Instance B: $b_{\text{Abs-Square,B}}[k] = \sum_{i=1}^{SB} \text{abs}(c_i'[k] + c_i'[k-1])^2$
– Hybrid XCorr algorithm related processing:
  Instance A: $b_{\text{XCorr,A}}[k] = \text{abs}(\sum_{i=1}^{SB-1} c_i'[k] \cdot c_{i+1}'^*[k])$
  Instance B: $b_{\text{XCorr,B}}[k] = \text{abs}(\sum_{i=1}^{SB-1} c_i'[k] \cdot c_{i+1}'^*[k] + c_i'[k-1] \cdot c_{i+1}'^*[k-1])$

Each instance uses its own threshold comparison step including threshold adaptation but the same scaling factor S is applied. A SF-detection is therefore reported if at least one of the two instances leads to a peak value above the threshold. Note that the improved $Pr(MP)$ by hybrid processing doubles the $Pr(FA)$ compared to the original approach.

In Fig. 3, we compare the $Pr(MP)$ performance for a CFO of $\nu = 0.01$, where the random sampling phase τ is assumed to be equally distributed over $\tau \in [-0.5, 0.5]$. Due to this randomness, Fig. 3 shows the mean $Pr(MP)$ which indicates averaging over τ. The worst-case roll-off of 5 % is considered and a configured target $Pr(FA) = 10^{-5}$ per each instance. Figure 3 shows a severe performance degradation compared to Fig. 2, where only $\tau = 0$ is valid. The hybrid processing (dashed curves) can improve the detection performance compared to the non-hybrid algorithms (solid curves) with a modest increase in
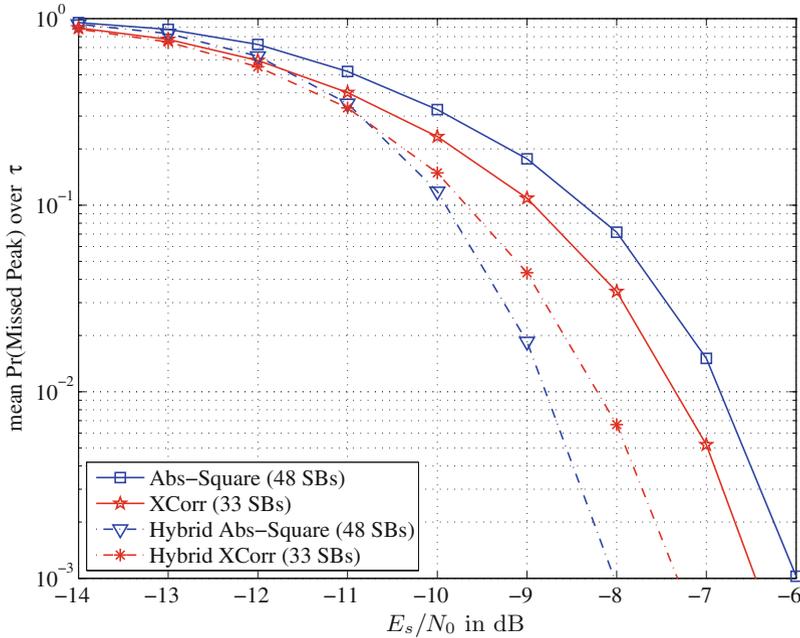

Fig. 3. Mean $Pr(MP)$ averaged over sampling phase offset τ versus E_s/N_0 for a CFO of $\nu = 0.01$ and roll-off 5 %.

the computation load. The Abs-Square approach benefits more from the hybrid processing than the XCorr approach, since the hybrid Abs-Square algorithm provides a gain of $2\,\mathrm{dB}$ in E_s/N_0 at mean $Pr(MP) = 10^{-3}$ compared to a hybrid XCorr gain of only $0.8\,\mathrm{dB}$. However, the hybrid XCorr has been selected for implementation because it inherently provides a CFO estimate.

3   Implementation of End-to-End Wideband Transmission

3.1   Testbed in the Laboratory

A hardware testbed has been developed that implements the DVB-S2X superframing using format 4 [13]. More specifically, the goal is to study, develop and validate the system and key technologies for the next generation of high-speed IP-based broadcasting and broadband access in future Ka band or Q/V bands satellite systems with wideband transponders. The overall structure of the wideband testbed is depicted in Fig. 4, where the involvement of companies is represented by their logos. It provides the following features and testing capabilities:

– End-to-End Multimedia Satellite Broadcasting System
– Demonstration of $> 1\,\mathrm{Gbit/s}$ over a single wideband transponder
– Proof-of-concept for multiplexing of different service types and QoS per stream
– Symbol Rates up to 400 Mbaud for future wideband transponders
– Support of a wide SNR range from $20\,\mathrm{dB}$ down to $-10\,\mathrm{dB}$
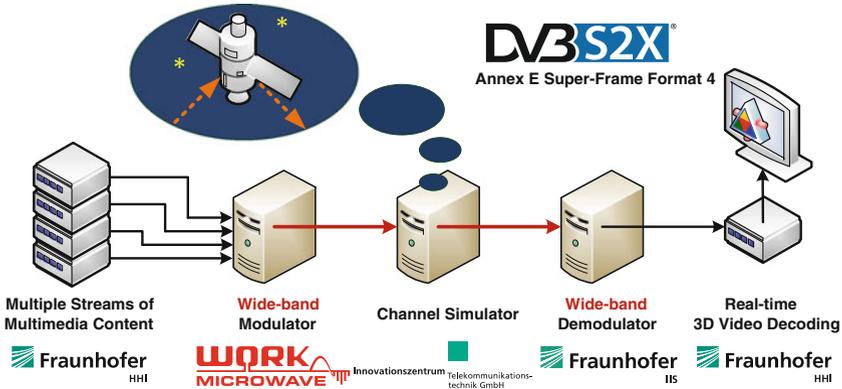– Realistic satellite channel models and impairments

Fig. 4. Visualization of the testbed for end-to-end wideband transmission.

Features of Key Components. The key components of the testbed are the wideband modulator and demodulator. The FPGA-based platform of the modulator relies on a newly developed board. In terms of wideband capabilities, the modulator supports high-speed multi-stream processing including prioritization schemes for different inputs:

– Up to 12 ASI inputs for transport streams with each 213 Mbit/s max data rate, which can be also internally reconfigured to TSoIP-to-TS converters
– Up to 4 integrated GSE Encapsulators with each up to 400 Mbit/s IP throughput

The demodulator platform combines a Xilinx Virtex 7 evaluation board VC707 and an ADC TI ADS5400EVM within the DT4950 industry PC. The demodulator supports time-slicing, where a subset of input streams can be selected at physical layer for simultaneous decoding and decapsulation. Robust synchronization methods are implemented for reliable operation down to -10 dB SNR.

Since both devices are compatible with the DVB-S2X specification implementing super-framing format 4, they support the complete roll-off range (5 %, 10 %, 15 %, 20 %, 25 %, 35 %) and all MODCODs related to QPSK, 8PSK, 16APSK, 32APSK for operation modes CCM, VCM, and ACM.

Furthermore, the channel simulator provides emulation of all effects of transmission over satellite with a signal bandwidth of up to 600 MHz. Apart from modeling satellite payload components like input/output filters or the non-linear amplifier and common implementation related impairments like phase-noise and frequency offset, rain-fading and mobility profiles can be applied to the signal.

Example Testbed Results. The test platform allows for live demonstration of broadcast transmission of advanced multimedia video/IPTV services. The wideband solution enables the transmission of a large number of channels and it supports high throughput applications such as 3DTV (Stereo at HD resolution) or multiple simultaneous HDTV resolutions (such as 720 p and 1080 p) or ultra HDTV. The receive side real-time video decoding directly reflects the impairments when QoS requirements of specific streams are not met due to worse channel conditions, e.g. switching back from 3D to 2D rendering. Moreover, the testbed allows analyzing the impact of all potential channel impairments as well as the gains due to activated counter-measures at receiver or transmitter. For example, increasing the symbol rate is limited w.r.t. the satellite filter characteristics and bandwidth introducing more and more inter-symbol interference. When applying signal equalization, the inter-symbol interference is compensated and the enhanced symbol rate directly yields increased throughput.

Examples of measurement results concerning this optimization of symbol rate R_s over transponder bandwidth B_{sat} and characteristics are shown in Fig. 5, where each point reflects the decoding threshold for a specific combination of symbol rate, roll-off, and MODCOD. Active channel impairments are satellite input/output filters and AWGN, wherefore the testbed achieves an overall implementation loss of only 0.2 to 0.3 dB w.r.t. the theoretical decoding thresholds (dashed vertical lines). One can observe for each MODCOD (colored boxes) that

driving the symbol rate and therefore the achieved spectral efficiency (relative to the transponder bandwidth) leads to degrading the decoding thresholds. Therefore, higher SNR values are required corresponding to a right-shift compared to the previous point of lower symbol rate. This is due to remaining inter-symbol interference and less received signal power because of attenuation at the band edges, which reflects the trade-off for symbol rate optimization.
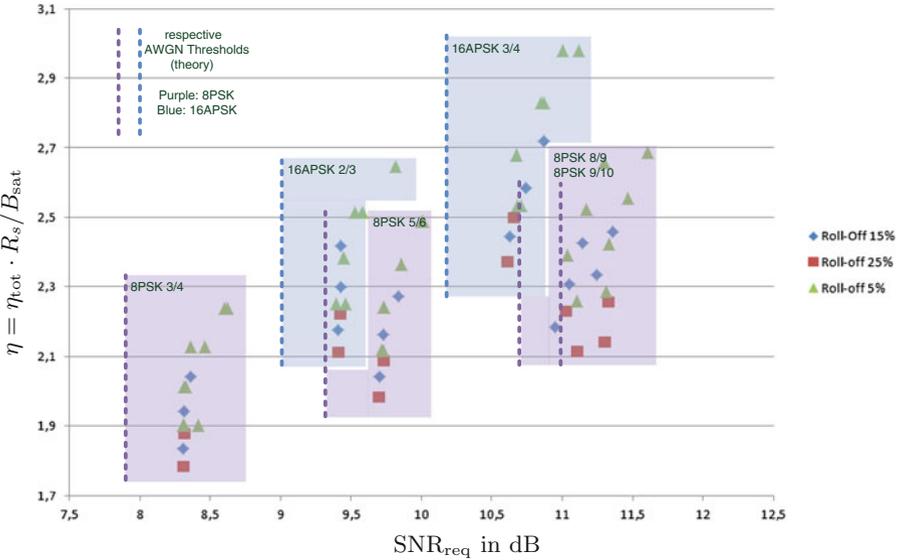

Fig. 5. Achieved spectral efficiency η relative to the satellite input/output filter bandwidth B_{sat} versus required SNR.

3.2   Planned Over-the-Air Tests

As an extension to the laboratory demonstration, an over-the-air live demonstration is also planned [14]. The main objective is to develop, integrate, verify and optimize further enhanced transmission techniques through testing over real-world wideband satellite transponders that allow for data rates over 1 Gbit/s on a single carrier per transponder transmission.

To achieve this goal, the testbed devices are further enhanced to support

– Higher order constellations (64APSK to 256APSK) according to the DVB-S2X specification
– Advanced static and dynamic predistortion techniques as well as enhanced equalization schemes
– Optimization of ACM algorithms, where the feedback loop from the receiver side to the gateway will be at IP level.

In order to qualify the availability and feasibility of a potential 1 Gbit/s link, various throughput analyses are carried out by means of link budget calculations, which depend on link impairments like weather condition statistics, satellite configuration like e.g. OBO optimization, and waveform configuration. Obviously, the final trade-off is between availability (target > 99.5 %) and net throughput on IP layer (target > 1 Gbit/s) for a given carrier.

In Fig. 6, simulation results for clear sky conditions show that the ambitious throughput targets are met in 31 % of the user locations in a beam footprint. More specifically, the 1080.7 Mbit/s physical data rate corresponds to 1019.4 Mbit/s IP data rate due to 2.67 % super-framing overhead and a 3 % worst-case GSE overhead. To achieve this, the HYLAS 2 satellite model is configured to have a carrier bandwidth of 230 MHz and 4 dB output back-off of the amplifier. For the transmit signal, the MODCOD 64APSK 5/6, a roll-off of 5 %, and a symbol rate of 219 Mbaud are used. Although these results hold for a user antenna size of 2.4 m, also tests with 1.2 m size are envisaged.
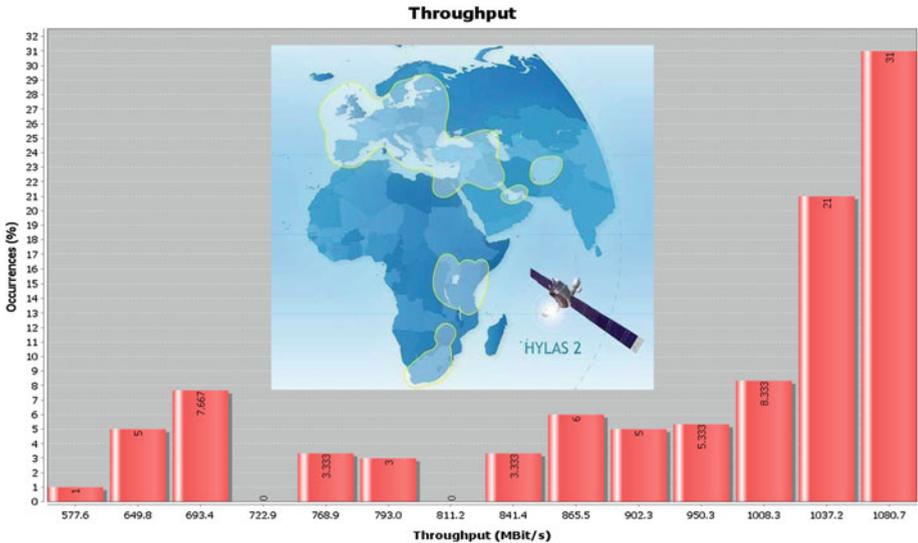

Fig. 6. Rate of throughput occurrence (derived from roll-off 5 % and different MODCODs) originating from randomly distributed user locations.

4   Conclusion

An introduction to the new SF format 4 of the DVB-S2X standard suitable for wideband transmission has been presented. This emphasizes that the superframe concept opens up possibilities to improve the flexibility and resilience to distortions as well as being future proof due to the super-frame content format signaling. Specifically, the configuration features of format 4, e.g., in terms of

scalability in SNR range have been shown. And simulation results have demonstrated the robustness of the waveform elements.

A hardware testbed has been established to validate the system and key technologies for the next generation of high-speed IP-based broadcasting and broadband access in future Ka band or Q/V bands satellite systems with wideband transponders, where symbol rates of up to 400 Mbaud are achieved and a wide SNR range from −10 to 20 dB is covered. As one example of a large variety of test and configuration cases, symbol rate optimization measurement results have been presented. Furthermore, early results for the planned over-the-air demonstration of wideband transmission show that transmission of 1 Gbit/s net data rate is feasible with the developed equipment.

References

1. ETSI EN 302 307–1 V1.4.1 (2014–11), Digital Video Broadcasting (DVB); Second generation framing structure, channel coding and modulation systems (...); Part 1: DVB-S2
2. Draft ETSI EN 302 307–2 (2014–10), Digital Video Broadcasting (DVB); Second generation framing structure, channel coding and modulation systems (...); Part 2: DVB-S2 Extension (DVB-S2X)
3. Draft ETSI TR 102 376–2 V1.1.1 (2014-xx), User guidelines for the second generation system for Broadcasting, Interactive Services News Gathering and other broadband satellite applications; Part 2: S2 eXtensions (DVB-S2X)
4. Digital Video Broadcasting (DVB), White Paper on the use of DVB-S2X for DTH applications, DSNG & Professional Services, Broadband Interactive Services and VL-SNR applications. DVB Document A172 (2015)
5. Caire, G., Debbah, M., Cottatellucci, L., De Gaudenzi, R., Rinaldo, R., Mueller, R., Gallinaro, G.: Perspectives of adopting interference mitigation techniques in the context of broadband multimedia satellite systems. In: 23rd AIAA International Communications Satellite Systems Conference (ICSSC), Rome (2005)
6. Angeletti, P., Fernandez Prim, D., Rinaldo, R.: Beam hopping in multi-beam broadband satellite systems: system performance and payload architecture analysis. In: 24th AIAA International Communications Satellite Systems Conference (ICSSC), San Diego (2006)
7. Proakis, J.G.: Digital Communications, 3rd edn. McGraw Hill Inc, New York (1995)
8. Scharf, L.: Statistical Signal Processing: Detection, Estimation, and Time Series Analysis. Addison Wesley, New York (1991)
9. De Gaudenzi, R., Giannetti, F., Luise, M.: Signal recognition and signature code acquisition in CDMA receivers for mobile communications. IEEE Trans. Vehic. Tech. **47**(1), 196–208 (1998)

10. Villanti, M., Salmi, P., Corazza, G.E.: Differential post detection integration techniques for robust code acquisition. IEEE Trans. Com. **55**(11), 2172–2184 (2007)
11. Gardner, F.M.: A BPSK or QPSK timing error detector for sampled receivers. IEEE Trans. Com. **COM–34**(5), 423–429 (1986)
12. Rohde, C., Stadali, H., Lipp, S.: Flexible Synchronization Concept for DVB-S2X Super-Framing in Very Low SNR Reception. Accepted for publication at Ka Conference, Bologna (2015)
13. European Space Agency Project, Wide-band Direct to Home (WiDiHo), Contract No. 4000103596/11/NL/AD. http://artes.esa.int/projects/wide-band-direct-home-widiho-itt6613
14. European Space Agency Project, Ultra-High Throughput Transmission Through Wideband Ka Transponder (TARGETS), Contract No. 4000110170/14/NL/EM